Generating novel waveguides for stimulated Brillouin scattering with genetic algorithms ⓕ

Jesper Håkansson ⓘ, and Dries Van Thourhout ⓘ

COLLECTIONS

Note: This article is part of the Special Topic "Optoacoustics − Advances in high-frequency optomechanics and Brillouin scattering" in APL Photonics.

ⓕ   This paper was selected as Featured

View Online   Export Citation   CrossMark

ARTICLES YOU MAY BE INTERESTED IN

Low-loss fiber-to-chip couplers with ultrawide optical bandwidth
APL Photonics 4, 010801 (2019); https://doi.org/10.1063/1.5064401

Realizing $Q >$ 300 000 in diamond microdisks for optomechanics via etch optimization
APL Photonics 4, 016101 (2019); https://doi.org/10.1063/1.5053122

Distributed opto-mechanical analysis of liquids outside standard fibers coated with polyimide
APL Photonics 4, 016105 (2019); https://doi.org/10.1063/1.5067271

Generating novel waveguides for stimulated Brillouin scattering with genetic algorithms Ⓕ

View Online   Export Citation   CrossMark

Jesper Håkansson ⓘD and Dries Van Thourhout ⓘD

AFFILIATIONS

Photonics Research Group, Ghent University and IMEC, Center for Nano- and Biophotonics, Technologiepark-Zwijnaarde 126, 9052 Ghent, Belgium

Note: This article is part of the Special Topic "Optoacoustics — Advances in high-frequency optomechanics and Brillouin scattering" in APL Photonics.

ABSTRACT

Over the last few years, there has been rapid development in demonstrating stimulated Brillouin scattering in chip-integrated optical waveguides. Most of the work has focused on finding good materials for achieving net gain, however, rather than on exploring novel waveguide designs. In this paper, we have used genetic algorithms to explore a wide range of possible waveguide shapes to achieve high gain in silicon and silicon oxide based integrated platforms. The result is a range of novel waveguide designs operating over a wide range of mechanical frequencies. Several of the waveguides found have a simulated gain in excess of 10^8 (Wm)$^{-1}$, far above anything previously demonstrated.

INTRODUCTION

Stimulated Brillouin scattering (SBS) in fibers has been known and analyzed for a long time. Often it presents an obstacle to the use of high optical powers in fibers,[1] but SBS also has been used as a platform for building various devices, e.g., lasers, strain sensors, RF synthesizers, and for four-wave mixing.[2–4] SBS in integrated photonics is still, however, a relatively new subject having been demonstrated only a few years ago.[5] Nevertheless, a host of promising applications like small footprint narrow linewidth lasers and tunable dynamic gratings[6–9] have already been demonstrated. To design a waveguide for high SBS gain, one needs to compromise between having a good optical waveguide, a good mechanical resonator, and a strong coupling between the two, all in the same physical structure. A related field, cavity optomechanics, has over the last decade experienced similar fast advances in performance and with that have come a myriad of new cavity designs.[10–12] In the field of SBS in integrated waveguides, however, the focus has been on investigating different waveguide materials while relying mostly on traditional waveguide shapes. It is far from obvious, however, that these are the optimal shapes and a whole range of possible waveguide shapes

remain almost entirely unexplored. To carry out that exploration, provide a wider range of possible waveguide shapes, and build an intuition as to what provides good coupling, we have turned to genetic algorithms.

Genetic algorithms (GA) are a class of general purpose search algorithms based on an iterative approach. The first step is to generate a population of samples. Then, in analogy to evolution, the next generation of samples is generated from the best performing samples of the current generation. By stepping forward generation by generation, passing on the best performing parameters, the algorithm converges towards a parameter set that optimizes the metric evaluated for. With this approach, GAs have been shown to often provide counterintuitive but educational answers in domains ranging from the growth of plants and website design to Othello strategies.[13–15]

The first part of this paper discusses how the GA utilized in our work is implemented. Important for the GA performance is how the waveguides (WG) are parameterized and evaluated as well as how the individual steps of the algorithm are implemented. The second part of the paper looks at some individual waveguides, focusing on the pareto-optimal designs, i.e., those providing the highest gain for a given

frequency, or simplified versions of these optimal designs. The third part of the paper focuses on the accumulated results of every simulated waveguide. It discusses the general trends and analyzes the pareto-frontier of the data generated. While the search space is not exhausted, the results obtained provide a way to benchmark a new waveguide in relation to the bulk of possible waveguides.

ALGORITHM

For a GA, there are typically five phases to consider: initial population, fitness function, selection, crossover, and mutation.

Our initial population consists of a selection of waveguides (WG) found in the literature, e.g., slot and ridge WGs, and a series of randomly generated rectangles. Each WG is represented by a matrix in which each element denotes a part of the cross section with an index corresponding to the material of that part; see illustration in Fig. 1(a). The area of each element is 50 nm × 50 nm, chosen because 50 nm is possible to the lithographically pattern. The parameters used for the algorithm are given in Table I. This rasterized approach is also attractive because it allows us the keep the same mesh for all simulations. However, the rasterization causes a problem for waveguides where two elements diagonal to each other are connected only in one of their corners. Such a connection is non-physical so any waveguide where such a connection is generated is removed and a new waveguide is generated. In order to speed up the simulations and as a proof of principle, this work focuses on forward SBS. Forward SBS requires far fewer simulation steps than backwards SBS where phase

TABLE I. The parameters of the genetic algorithm.

Size, waveguide	17 × 14 elem.
Area, element (nm)	50 × 50
FEM mesh	Triangular
FEM mesh resolution	12 nodes per element
Materials	Si, SiOx, and air
Size, population	100
Size, selection	50
Probability, mirror mutation (%)	15
Probability, reassign mutation (%)	15
Simulated waveguides, total	24 000

matching requires simulation of several mechanical propagation vectors. As a result of limiting the simulation to forward SBS, the mechanical waves do not propagate along the waveguide and beam modes are not possible.

The waveguides are assumed to be suspended and the substrate is assumed to be far enough to be not relevant for the optical simulation. Such a waveguide would need to be periodically suspended but, as in forward SBS the mechanical waves do not propagate, it is a good approximation to treat the suspended sections as mechanically independent from the anchoring sections.[16]

The main factor determining the fitness function used to evaluate the waveguide is the Brillouin gain. The gain is calculated from optical and mechanical mode simulations using COMSOL Multiphysics from which the mode overlap is then calculated via MATLAB scripting. The simulated waveguide matrix is centered in a circular area of air with 3 μm radius and Robin boundary conditions with a complex coefficient. The gain function is given by[17]

$$G = \frac{2\omega_{opt}Q_{mech}|\langle \mathbf{f}, \mathbf{u}\rangle|^2}{v_{group}^2 \omega_{mech}^2 m_{eff}}, \qquad (1)$$

where ω_{mech}, Q_{mech}, and m_{eff} denote, respectively, the mechanical frequency, the quality factor, and the effective mass. ω_{opt} and v_{group} are the optical frequency and the group velocity. The effective mass is calculated from $m_{eff} = \iint_A \rho|\mathbf{u}|^2 dA$ where $\mathbf{u}$ is the mechanical displacement field and ρ is the density of the material. The integral is taken over the waveguide cross section, A. The mechanical displacement is normalized to its maximum, $\max|\mathbf{u}| \equiv 1$. The term $\langle \mathbf{f}, \mathbf{u}\rangle/v_{group}$ denotes the power normalised optomechanical force driving the vibration whereby,

$$\langle \mathbf{f}, \mathbf{u}\rangle = \langle \mathbf{f}, \mathbf{u}\rangle_{RP} + \langle \mathbf{f}, \mathbf{u}\rangle_{ES}$$
$$= \oint_S \frac{1}{2}(\epsilon E_\parallel^2 + \epsilon_{inv}D_\perp^2)(\hat{n} \cdot \mathbf{u})\,dS + \iint_A \frac{1}{2}n^4\mathbf{E}_i\mathbf{E}_j p_{ijkl}S_{kl}\,dA \qquad (2)$$

with $\mathbf{E}$ and $\mathbf{D}$ the electrical field and the electrical displacement field, respectively.

The first term denotes the radiation pressure, which is calculated as a line integral along the interface between the different materials of the waveguide, whereby ϵ and ϵ_{inv} are the difference in permittivity and inverse permittivity between the two materials at the interface. The subscripts $\parallel$ and $\perp$ denote the field parallel and orthogonal to the interface. $\hat{n}$ is
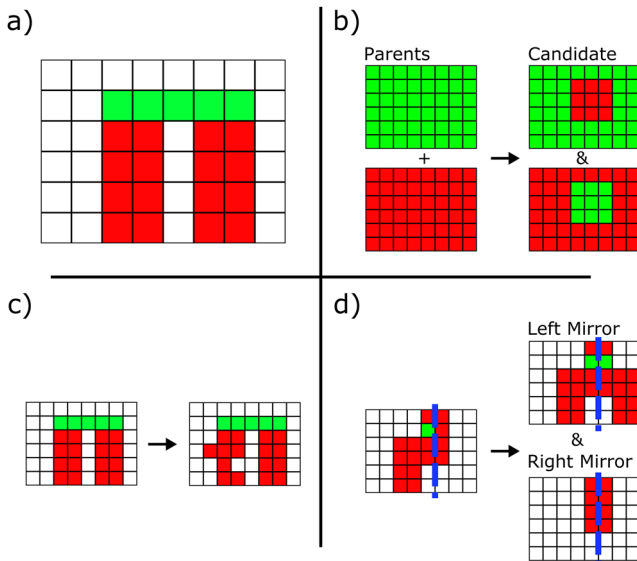

FIG. 1. (a) The waveguide matrix with three colors marking three materials. (b) The crossover phase that generates new waveguides. The mutation phase that maintains diversity by introducing a change in the current populations with (c) a reassign mutation and (d) a mirror mutation.

TABLE II. Mechanical and optical material constants.[18,19] C_{ij} are constants of the elastic tensor. For silicon, the values are calculated for the ⟨110⟩ orientation. The oxide is isotropic so p_{44} and p_{66} are calculated from the other values.

Material	C_{11} [GPa]	C_{12} [GPa]	C_{13} [GPa]	C_{33} [GPa]	C_{44} [GPa]	C_{66} [GPa]	ρ [kg/m³]	p_{11}	p_{12}	p_{13}	p_{33}	p_{44}	p_{66}	n_{eff}
c-Si	195	35	64	166	80	51	2329	−0.0968	0.0052	0.0094	−0.101	−0.051	−0.0552	3.47
SiO$_x$	78.6	16.1	16.1	78.6	31.2	31.2	2203	0.121	0.271	0.271	0.121	−0.075	−0.075	1.48

the normal to the material interface. The electric power is normalized to $\iint_N |\mathbf{ED}^*| dN \equiv 1$. This integral is taken over the full plane perpendicular to the waveguide.

The second term, which denotes the contribution due to electrostriction, is calculated as an integral over the cross section of the WG. p_{ijkl}, S_{kl}, and n are the photoelastic tensor, strain, and refractive index.

The material constants used are shown in Table II and where taken from the literature.[18,19] They were rotated to the crystal orientation ⟨110⟩, commonly used in silicon photonics.

The simulation software first generates a set of optical and mechanical modes and then calculates the optomechanical forces and the resulting gain for each mode pair. The gain function benefits so significantly from lowering the mechanical frequency that in order to generate individuals of a higher frequency, we chose to introduce a higher order band-pass filter. The fitness function used to calculate the fitness score is

$$F_{func} = G \frac{\omega_{mech}^{2.5}}{(\omega_{mech} - \omega_{filt})^2 + (\omega_{mech}/Q_{filt})^2}, \quad (3)$$

where ω_{filt} is the central frequency of the filter and Q_{filt} dictates the width of the filter. A Q_{filt} of 3 was found to be good enough for this work.

The selection step decides the group of WGs from which the next generation is generated. The method used in this work is elitist, meaning the samples with the highest ever fitness score are selected for the future steps of the algorithm. Regardless of whether they are selected or not, all samples are saved for future reference.

The crossover phase is where a new generation is made. From the selected samples, new samples are generated until the population is once again as large as it should be. To generate a new pair of samples, two parent samples are randomly chosen from the group of selected WGs. A rectangular part of the two parents is swapped resulting in two new samples, one mostly like parent A with a bit of B and the other B with a bit of A; see Fig. 1(b).

The mutation phase consists of two cases: a probability that a few elements in the WG matrix are randomly reassigned, see Fig. 1(c), and a probability that the WG is mirrored across a randomly located axis; see Fig. 1(d). The mirror mutation generates two samples, one from the right side of the axis and one from the left side. This mutation benefits symmetric WGs, which are the most represented among the WGs in which SBS has already been demonstrated experimentally.

The new population is then evaluated according to the fitness function, the best scoring samples are selected for the next generation and the loop continues. When there is no

change in the sample with the highest fitness score over a few generations, the algorithm has run its course.

When the GA has converged, the stored data can be reused to find an optimum at a new mechanical frequency. The computationally expensive part of evaluating the fitness function is the calculation of the overlap integral ⟨**f**, **u**⟩, which is independent of the filter frequency and hence does not have to be recalculated. Therefore the existing set of data can be used as a starting point and within a few generations, the algorithms now converge to a new optimum. This means that each subsequent cycle can be sped up by an ever larger database of WGs to start from.

Another important parameter to be set is the mechanical quality factor. In the waveguide structures, we consider in this work, the mechanical losses are typically not dominated by clamping losses or air damping (which can be removed in vacuum). More often they are limited by other factors, which are difficult to take into account directly in the simulations. Therefore we choose to fix the mechanical quality factor to Q_{mech} = 1000. This is roughly the same value as has been measured in suspended wire WGs and has been used for these kind of simulations in the past.[17,20] As we will elaborate further, this is a conservative choice, in particular, at lower frequencies but does not influence the major conclusions of the paper.

INDIVIDUAL RESULTS

Figure 2 shows the gain plotted against mechanical frequency of all the mode pairs generated. It also marks a few selected modes, which are displayed in detail in Table III. The
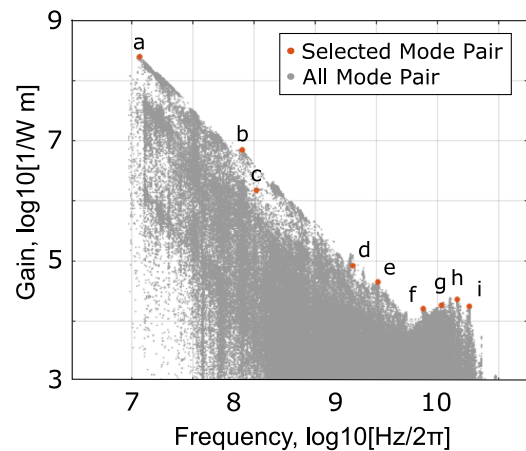

FIG. 2. The gain and frequency of all simulated mode pairs. The modes and waveguides selected in Table III are indicated by the dots labeled a–i.

TABLE III. A selection of competitive, distinct, and noteworthy waveguides. They are indicated in Fig. 2 with red points. Shown, starting from the left, in each row are material composition and shape, mechanical mode, optical mode, and simulated performance. The shape is shown on top of a 50×50 nm grid. ES and RP are the electrostrictive and radiation pressure force. The forces are in all the given examples interfering constructively.
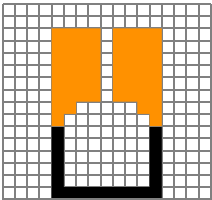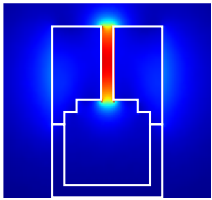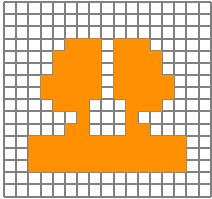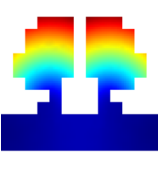
INDIVIDUAL MODES			
Shape Orange: Si Black: SiOx	Mechanical Displacement 0 ▭ 1	Optical Amplitude 0 ▭ 1	Simulated performance

(a)

Gain: 2.5×10^8 (1/Wm)

Freq.: 37 (MHz)	Eff. Mass: 169 (ng/m)
Eff.Ind.: 1.50	Group Ind.: 3.14
RP: 29.9 (mN/Wm)	ES: 217 (nN/Wm)

(b)
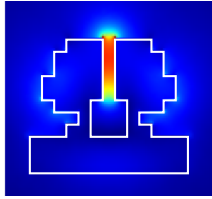
Gain: 7.0×10^6 (1/Wm)

Freq.: 253 (MHz)	Eff. Mass: 103 (ng/m)
Eff.Ind.: 1.34	Group Ind.: 3.95
RP: 27.1 (mN/Wm)	ES: 39.2 (μN/Wm)

(c)
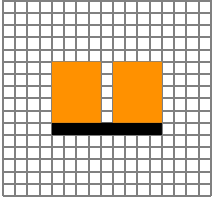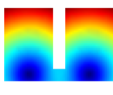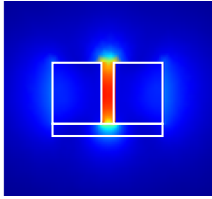
Gain: 1.5×10^6 (1/Wm)

Freq.: 330 (MHz)	Eff. Mass: 85.3 (ng/m)
Eff.Ind.: 1.38	Group.Ind.: 2.87
RP: 15.0 (mN/Wm)	ES: 10.1 (μN/Wm)

(d)
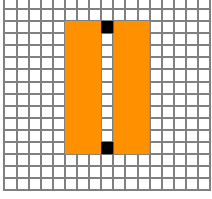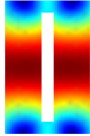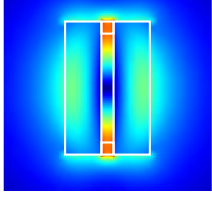
Gain: 8.4×10^4 (1/Wm)

Freq.: 2.04 (GHz)	Eff. Mass: 191 (ng/m)
Eff.Ind.: 1.25	Group Ind.: 4.69
RP: 29.9 (mN/Wm)	ES: 2.86 (mN/Wm)

(e)
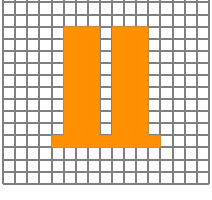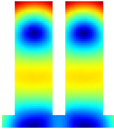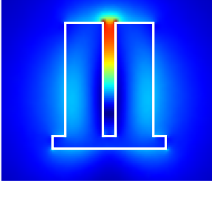
Gain: 4.5×10^4 (1/Wm)

Freq.: 3.27 (GHz)	Eff. Mass: 91 (ng/m)
Eff.Ind.: 1.17	Group Ind.: 5.03
RP: 22.7 (mN/Wm)	ES: 3.90 (mN/Wm)

(f)
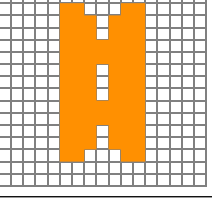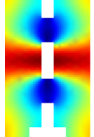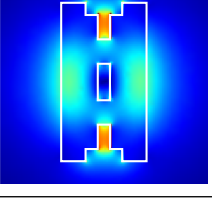
Gain: 1.6×10^4 (1/Wm)

Freq.: 7.68 (GHz)	Eff. Mass: 163 (ng/m)
Eff.Ind.: 1.50	Group Ind.: 4.74
RP: 27.0 (mN/Wm)	ES: 23.1 (mN/Wm)

TABLE III. (*Continued*.)

		INDIVIDUAL MODES	
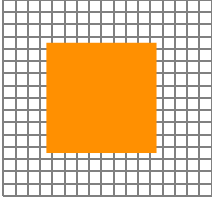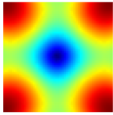
(g)　Gain: 1.9×10^4 (1/Wm)

Freq.: 10.8 (GHz)　　　　　Eff. Mass: 203 (ng/m)

Eff.Ind.: 1.31　　　　　　　Group Ind.: 8.58

RP: 70.9 (mN/Wm)　　　　ES: 13.6 (mN/Wm)
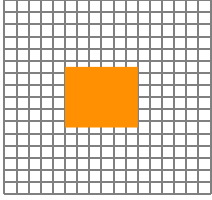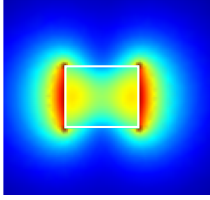
(h)　Gain: 2.3×10^4 (1/Wm)

Freq.: 14.6 (GHz)　　　　　Eff. Mass: 154 (ng/m)

Eff.Ind.: 1.56　　　　　　　Group Ind.: 5.75

RP: 49.0 (mN/Wm)　　　　ES: 26.9 (mN/Wm)
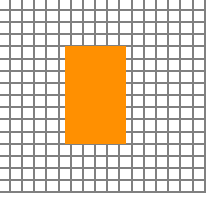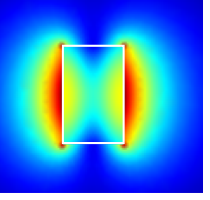
(i)　Gain: 1.8×10^4 (1/Wm)

Freq.: 18.3 (GHz)　　　　　Eff. Mass: 91.5 (ng/m)

Eff.Ind.: 1.44　　　　　　　Group Ind.: 5.57

RP: 75.6 (mN/Wm)　　　　ES: 18.5 (mN/Wm)

mode pairs can be segmented in different types by looking at the parameters of the mode pair, e.g., the mode order, group velocity, and effective mass. It is by sorting through the data, identifying the best performing, and most distinct or most simple WGs that the authors have selected the subset of WGs, denoted a-i in Fig. 2 and Table III, to focus on.

The highest gain mode pairs are found at the lowest frequencies simulated. Of those, the highest gain is generated by WG (a), as shown in Fig. 2 and Table III. It is a slot WG where the optical mode is forced into the space between two high refractive index sections.[21] The field being confined in the air slot is beneficial in two ways: the associated radiation pressure is high and air is less optically nonlinear than silicon, allowing for the use of high optical powers. In this case, the two WGs are mechanically connected by a soft spring. The spring is made from oxide as silicon is stiffer, which would increase the mechanical frequency. Such an intricate mechanical connection makes fabrication difficult however. By radically simplifying the connection we arrived at WG (c). While in this waveguide the coupling is worse than, e.g., WG (a), it is easier to fabricate and still has a higher gain than anything previously demonstrated.

There is also a group of highly competitive structures, which involves higher order optical modes. For these WGs, the slot is situated above and connected to a slab of silicon. By introducing a high refractive index in the proximity of a slot that can guide a higher order slot mode, the degeneracy of the mode is broken and it splits up. This leaves modes, e.g., in WG (b) and WG (e), where the electric field is confined mostly in the top part of the slot where it is overlapping well with the mechanical mode.

A way to avoid disturbing the optical mode with the mechanical connection is to have an identical connection on both sides, e.g., WG (d). This has the added benefit that it confines the mechanical mode such that the overlap of optical power and mechanical motion is better. It does, however, also unfortunately add some effective mass to the mode. Overall these mode combinations still result in a relatively high gain.

WG (f) demonstrates yet another type of mechanical connection. By moving the connecting parts towards the center, the optical field in the slot now results in a significant radiation pressure that has the same phase as the electrostriction. As such, these forces can constructively add up to a respectable gain for the given frequency.

It is also possible to increase the forces by increasing the group index. A waveguide near the cutoff of an optical mode is usually more sensitive to the wavelength, which in turn results in a large group index. Designing for that effect leads to waveguides such as WG (g), which support higher order modes with very high group index.

Finally, the highest frequency range is populated by lamb wave modes, WG [(h) and (i)]. These modes are the ones that are most common among the integrated SBS WGs already demonstrated in the literature, such as wire WGs.[16]

So far missing from our discussion in this paper are ridge WGs[7] and double slots.[22] Ridge WGs are used mainly because they can have very low optical losses, something that is difficult to include in the optimization process. They do however have a worse SBS coupling, which leaves the gain below the pareto-curve. Double slots do not support forward SBS as the forces in both slots pull equally on the center beam but in opposite directions and as such the forces cancel itself. The net forces suggested in Ref. [22] come from inter-modal SBS where the overlap between a symmetric and an asymmetric optical mode change the sign of the force on one side of the symmetry line, summing up to a substantial force.

GLOBAL RESULTS

Looking at the collection of all the simulated results, it is possible to see some more general trends and limits. Figure 4 shows the gain as function of frequency. The color indicates the group index of the optical mode in the selected mode pair and the results are sorted so a higher group index will cover a lower one. This graph shows that the mode pairs with the highest gain do not have a high group index despite the advantages implied in the gain equation, Eq. (1). This indicates other factors are dominating the gain, which is partly explained by the fact that the group index overall only varies over a relatively limited range and the highest group index waveguides are typically near cutoff and hence not well confined. The highest gain waveguides, e.g., WG (a), are, as mentioned earlier, slot waveguides, which, although they have a slightly lower group index, benefit from very strong radiation pressure coupling and low stiffness.

Manually designing slot WGs with lower mechanical frequencies shows that the trend continues but it yields an increasingly unlikely shape for the GA to generate. Since WGs such as (a) have almost no electrostrictive coupling and the part of the waveguide deciding the stiffness of the mechanical mode does little to affect the optical mode it is convenient to separate the frequency from the gain function. By multiplying the gain with the frequency squared we get a frequency independent gain, which can be used as a benchmark for the other WGs. To do so, and since the mechanical stiffness is dictated by parts outside of the optical mode, we neglect the mechanical interaction. We assume the mechanical mode is just a modulation of the slot width and re-express the two sides of the slot as polygons instead of as pixels. We can then use a gradient descent method for each vertex of the polygon to converge to a local optimum, illustrated in the inset of Fig. 4, with a frequency normalized gain of $k_{opt} = 1.45 \times 10^{25}$ m^{-1} W^{-1} s^{-2}, as displayed relative to the rest of the data in Fig. 4. With the k_{opt}-curve as a reference, it is now visible which waveguides exceed it. A majority of these are concentrated at higher frequencies.

Figure 3 zooms in on the relative contribution of the radiation force and the electrostriction. Figure 3(a) shows the two force components with the color gradient marking the gain. The trend in the data is that for a high gain, strong radiation pressure coupling is paired with a very weak electrostrictive coupling. Achieving a high electrostrictive coupling at a low frequency is difficult. This is because the mechanical frequency depends on the ratio of stiffness to effective mass. The stiffness in turn depends on the strain of the mechanical mode normalized to the same point as the effective mass and the Young's modulus. Finally the strain then couples to the optical mode via the electrostrictive constant, so the electrostrictive force depends on an optical overlap with the same strain the mechanical frequency depends on. Altogether it means that a strong electrostrictive coupling becomes more difficult to achieve the lower the frequency is; see Fig. 3(b). The radiation pressure, however, is not as dependent on mechanical frequency, see Fig. 3(c), and can be strong in lower frequency WGs.

The electrostrictive contribution is maximized in the high frequency region, where the highest gain is obtained for variations of wire WGs. The good coupling is due to the good overlap between the optical mode and the strain distribution of the mechanical mode as well as the high stiffness. The optomechanical coupling is improved further by a very good radiation pressure coupling. As a consequence, several of these waveguides rise well above the black k_{opt}-curve and the frequency dependent trend set by lower frequencies.

Figure 4 also shows that it is difficult to get a good gain above 20 GHz. This is because the mechanical frequency is increased either by using smaller WGs, where less of the light is confined in the semiconductor, or by using a higher order mechanical mode, which has a worse overlap with the
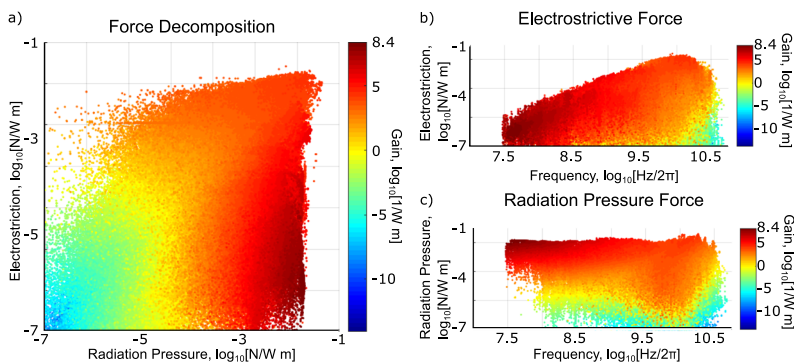

FIG. 3. The separate power-normalized force components: (a) relative to each other as well as (b) electrostriction and (c) radiation pressure separately. The color signifies the highest gain found at the indicated place in the graph.
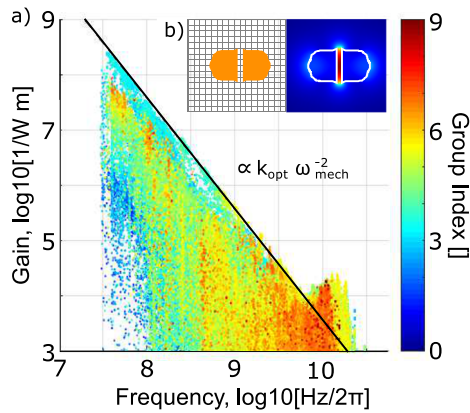
FIG. 4. (a) The gain, frequency, and group index of all simulated mode pairs. The black line indicates the frequency normalized gain of the optimized slot waveguide shown in the inset. The mechanical quality factor is set to 1000. (b) Silicon slot waveguide optimized for highest gain assuming horizontal movement and the associated optical mode. Each square in the grid pattern is 50×50 nm.

optical mode. In both cases, the optomechanical coupling decreases.

As explained above, we choose to fix the mechanical quality factor at a value Q_{mech} = 1000 as the real value cannot be calculated with sufficient accuracy. Mechanical losses in waveguide structures as the ones used here are often limited not only by air damping, which is removed in vacuum, and surface oxide, which can be reduced through optimized fabrication, but also by thermal material properties like Akhiezer and thermoelastic damping, which can be reduced by cooling. Ultimately it seems that the limit for the mechanical quality factor is inversely proportional to the mechanical frequency,[23] favouring the low frequency structures. This suggests the gain could be significantly higher for the low frequencies than our simulated results imply. The main conclusions of the work are not affected by this choice, however.

CONCLUSIONS

The goal of this study was to use genetic algorithms to find new competitive waveguide geometries. Several thousands of waveguides have been simulated and many previously not suggested waveguides have been found and analyzed. As can be expected, slot waveguides where the mechanics and the optics can be separated are the best performing waveguides in the lower frequency range. However, several variations of the slot waveguide design have been shown to have their own advantages. Some slot waveguides exhibit a high group index, others have high electrostrictive coupling or by designing for a higher order optical mode allow to tailor the mode for a high coupling and a lower effective mass. We show several waveguides that have a gain exceeding 10^8 1/Wm, well above any previously demonstrated SBS WG. For higher frequencies, wire WGs take over and generate the highest gain as they have a better optical overlap

with the strain resulting in a much stronger electrostrictive coupling.

A potential next step to improve on the algorithmic approach for finding new WGs is to include a novelty score in the selection procedure.[24] It has been shown to generate very competitive results for complex problems when not starting near a global maximum.

Initial tests also show it is possible to generate high gain waveguides for inter-modal SBS. However, due to the increased non-linearity of the problem, convergence is slower.

REFERENCES

[1]E. Garmire, R. Chiao, and C. Townes, "Dynamics and characteristics of the self-trapping of intense light beams," Phys. Rev. Lett. **16**, 347 (1966).

[2]K. Hill, B. Kawasaki, and D. Johnson, "cw Brillouin laser," Appl. Phys. Lett. **28**, 608–609 (1976).

[3]A. Scott and K. Ridley, "A review of Brillouin-enhanced four-wave mixing," IEEE J. Quantum Electron. **25**, 438–459 (1989).

[4]T. Schneider, D. Hannover, and M. Junker, "Investigation of Brillouin scattering in optical fibers for the generation of millimeter waves," J. Lightwave Technol. **24**, 295 (2006).

[5]R. Pant, C. G. Poulton, D.-Y. Choi, H. Mcfarlane, S. Hile, E. Li, L. Thevenaz, B. Luther-Davies, S. J. Madden, and B. J. Eggleton, "On-chip stimulated Brillouin scattering," Opt. Express **19**, 8285–8290 (2011).

[6]M. Merklein, A. Casas-Bedoya, D. Marpaung, T. F. Büttner, M. Pagani, B. Morrison, I. V. Kabakova, and B. J. Eggleton, "Stimulated Brillouin scattering in photonic integrated circuits: Novel applications and devices," IEEE J. Sel. Top. Quantum Electron. **22**, 336–346 (2016).

[7]N. T. Otterstrom, R. O. Behunin, E. A. Kittlaus, Z. Wang, and P. T. Rakich, "A silicon Brillouin laser," Science **360**, 1113–1116 (2018).

[8]R. Pant, E. Li, C. G. Poulton, D.-Y. Choi, S. Madden, B. Luther-Davies, and B. J. Eggleton, "Observation of Brillouin dynamic grating in a photonic chip," Opt. Lett. **38**, 305–307 (2013).

[9]I. V. Kabakova, R. Pant, D.-Y. Choi, S. Debbarma, B. Luther-Davies, S. J. Madden, and B. J. Eggleton, "Narrow linewidth Brillouin laser based on chalcogenide photonic chip," Opt. Lett. **38**, 3208–3211 (2013).

[10]A. Schliesser, P. DelHaye, N. Nooshi, K. Vahala, and T. Kippenberg, "Radiation pressure cooling of a micromechanical oscillator using dynamical backaction," Phys. Rev. Lett. **97**, 243905 (2006).

[11]M. Eichenfield, J. Chan, R. M. Camacho, K. J. Vahala, and O. Painter, "Optomechanical crystals," Nature **462**, 78 (2009).

[12]J. Thompson, B. Zwickl, A. Jayich, F. Marquardt, S. Girvin, and J. Harris, "Strong dispersive coupling of a high-finesse cavity to a micromechanical membrane," Nature **452**, 72 (2008).

[13]J. C. Quiroz, S. J. Louis, A. Shankar, and S. M. Dascalu, "Interactive genetic algorithms for user interface design," in *IEEE Congress on Evolutionary Computation (CEC), 2007* (IEEE, 2007), pp. 1366–1373.

[14]L. Xu, M. Tao, and H. Ming, "A hybrid algorithm based on genetic algorithm and plant growth simulation algorithm," in *International Conference on Measurement, Information and Control (MIC), 2012* (IEEE, 2012), Vol. 1, pp. 445–448.

[15]J.-M. Alliot and N. Durand, "A genetic algorithm to improve an othello program," in *European Conference on Artificial Evolution* (Springer, 1995), pp. 305–319.

[16]R. Van Laer, B. Kuyken, D. Van Thourhout, and R. Baets, "Interaction between light and highly confined hypersound in a silicon photonic nanowire," Nat. Photonics **9**, 199 (2015).

[17]W. Qiu, P. T. Rakich, H. Shin, H. Dong, M. Soljačić, and Z. Wang, "Stimulated Brillouin scattering in nanoscale silicon step-index waveguides: A general framework of selection rules and calculating SBS gain," Opt. Express **21**, 31402–31419 (2013).

[18]G. Simmons and H. Wang, *Single Crystal Elastic Constants and Calculated Aggregate Properties: A Handbook* (MIT Press, Cambridge, MA, 1971).

[19]A. Yariv and P. Yeh, *Optical Waves in Crystals* (Wiley, New York, 1984), Vol. 5.

[20]R. Van Laer, B. Kuyken, D. Van Thourhout, and R. Baets, "Analysis of enhanced stimulated Brillouin scattering in silicon slot waveguides," Opt. Lett. **39**, 1242–1245 (2014).

[21]V. R. Almeida, Q. Xu, C. A. Barrios, and M. Lipson, "Guiding and confining light in void nanostructure," Opt. Lett. **29**, 1209–1211 (2004).

[22]R. Van Laer and A. Safavi-Naeini, "Enabling strong coupling in nanoscale silicon optomechanical waveguides," in *Conference on Lasers and Electro-Optics (CLEO)*, 2017 (IEEE, 2017), pp. 1–2.

[23]S. Ghaffari, S. A. Chandorkar, S. Wang, E. J. Ng, C. H. Ahn, V. Hong, Y. Yang, and T. W. Kenny, "Quantum limit of quality factor in silicon micro and nano mechanical resonators," Sci. Rep. **3**, 3244 (2013).

[24]J. Gomes, P. Mariano, and A. L. Christensen, "Devising effective novelty search algorithms: A comprehensive empirical study," in *Proceedings of the 2015 Annual Conference on Genetic and Evolutionary Computation* (ACM, 2015), pp. 943–950.